RSC Advances

PAPER

Cite this: *RSC Adv.*, 2020, **10**, 38861

Efficient NIR energy conversion of plasmonic silver nanostructures fabricated with the laser-assisted synthetic approach for endodontic applications

Tetiana Bulavinets, *[a] Magdalena Kulpa-Greszta,[b] Agata Tomaszewska,[c] Malgorzata Kus-Liśkiewicz,[c] Gabriela Bielatowicz,[c] Iryna Yaremchuk,[a] Adriana Barylyak,[d] Yaroslav Bobitski[ae] and Robert Pązik [c]

Received 17th July 2020
Accepted 7th October 2020

DOI: 10.1039/d0ra06614a

rsc.li/rsc-advances

Silver nanoparticles were synthesized with the laser-assisted wet chemical approach at room temperature. The effect of light exposure on the silver nanoparticles' spatial parameters shaping the localized surface plasmon resonance has been evaluated. The optical, structural and morphological characterizations of the Ag nanostructures were conducted with UV-VIS-NIR spectrophotometry, DLS and TEM techniques. The ability of the light-modified Ag nanostructures for energy conversion under the influence of 445 and 880 nm laser radiation is estimated. We have found that the most efficient heat generation can be achieved using triangular Ag nanostructures under the NIR irradiation (880 nm). The temperature effect on the Ag nanostructures' antibacterial properties has been evaluated against the *Staphylococcus aureus* population. The prospects of triangular Ag nanostructures' application on modern endodontics for the rapid nano-laser disinfection of the root canal system of the human tooth have been demonstrated.

Introduction

The fast development of nanotechnology and continuous improvement of synthetic approaches towards nanomaterials characterized by the specific and controlled shape, size, structural and physicochemical properties have led to the extension of their possible application in various fields of engineering, energetics, photonics, plasmonics, ecology and other important directions.[1] Nowadays, trials with implementation of nanomaterials in broadly understood biomedicine, for instance, periodontics, endodontics, early stage diagnosis, theranostics, temperature controlled drug release and stimulation of regenerative processes or even localized hyperthermia, are extremely promising.[2–4] The study of the behaviour of nanoscale metal structures, in particular silver, is of great importance for the aforementioned purposes[5,6] due to its unique physicochemical, biological, catalytic and bactericidal properties.[7–10] These properties are especially manifested under the conditions of localized surface plasmon resonance (LSPR).[11] The LSPR effect is characterized by a sharp increase in the optical absorption and scattering of the electromagnetic radiation by nano-objects at a certain wavelength of the incident light, which resonates with the eigen frequency of electron gas oscillations on the metal nanoparticle surface.[12] Thus, engineering metallic nanoparticles with controlled spatial parameters besides the maximized optical response of the given nanostructures, especially within the range known as a biological optical window, is a primary objective and will critically depend on the synthetic approach.[7] Preferably, the LSPR peak of the Ag nanostructures must be located in the spectral range where the electromagnetic wave has maximal ability to penetrate the irradiated tissue for theranostic applications. Typically, the plasmonic absorption peaks of Ag nanoparticles (Ag-NPs) can be found between 390 and 450 nm, which in turn, drastically limits their use in biological systems.[13] However, this drawback can be overcome by the modification of the Ag plasmonic properties and their LSPR through the careful control of the nanoparticles' spatial parameters (size, shape and structure)[14,15] or properties of the surrounding medium.[16] For instance, plasmonic gold and silver nanomaterials have been explored for treating cancer by photothermal ablation therapy.[17] This approach is based on the nanoparticles' heat generation from light for destroying cancer cells, and requires high optical absorption and strong photothermal conversion efficiency. Triangular silver nanoprisms were also used as coatings for the dental implants to enhance osteointegration after implantation surgery by reducing post-implantation infection. It was shown that the Ag triangular

[a]*Department of Photonics, Lviv Polytechnic National University, S. Bandera Str. 12, 79013 Lviv, Ukraine. E-mail: tetiana.o.bulavinets@lpnu.ua*
[b]*Faculty of Chemistry, Rzeszow University of Technology, Aleja Powstańców Warszawy 12, 35-959 Rzeszow, Poland*
[c]*Department of Biotechnology, Institute of Biology and Biotechnology, College of Natural Sciences, University of Rzeszow, Pigonia 1, 35-310 Rzeszow, Poland*
[d]*Department of Therapeutic Dentistry, Danylo Galytsky Lviv National Medical University, Pekarska Str., 69, 79010 Lviv, Ukraine*
[e]*Department of Physics, Centre of Microelectronic and Nanotechnology, College of Natural Sciences, University of Rzeszow, Pigonia 1, 35-310 Rzeszow, Poland*

nanoprisms have higher antibacterial activity in comparison to spherical ones.[18]

One of the most effective techniques that allows for precise control of the optical characteristics of Ag nanoparticles through modification of their spatial parameters relies on the utilization of electromagnetic irradiation.[19] This is a very useful approach in exploiting the property of general nano-objects, namely their ability to absorb specific wavelengths.[20] The advantage of the laser radiation is coherence, monochromaticity, directionality and high intensity. These features allow resonant effects on the starting reagents and products of chemical reactions to occur. Thus, it provides accurate and precise localization, dosage, absolute sterility and a high rate of energy input into the reaction zone. Therefore, it is possible to focus the laser beam on the nanoscale plane and localize chemical transformations on the nanoscale.[21] The photochemical effect is manifested in the occurrence of the chemical activity of atoms and molecules as a result of direct photon absorption. This is most easily observed when the electronic states of atoms and molecules are excited with laser radiation in the visible range since the activation energy of a chemical reaction is usually high.[22] Therefore, photoinduced recovery allows for obtaining the time-stable metal nanoparticle colloids, which have certain advantages in comparison with nanostructures obtained with other wet-chemical techniques. Light is the purest and almost non-toxic tool for the formation of silver nanostructures due to their ability to absorb radiation with a certain wavelength. Moreover, the ease of controlling the chemical processes in time and space is possible. This cannot be achieved in other approaches utilizing thermodynamically and kinetically unstable systems.

Sodium citrate ($Na_3C_6H_5O_7$) is the most commonly used capping agent to obtain stable colloidal suspensions of Ag-NPs. This is due to its proven non-toxic properties, namely, as a widely approved food and pharmaceutical additive treated as a safe compound. This agent does not participate in the reduction of silver ions, and acts only as a stabilizer since photoinduced synthesis occurs at room temperature. Conversely, in the Turkevich method,[23] it serves as the Ag^+ reducer and is responsible for the good stability of Ag nanoparticles in the solution. However, this process is carried out at a higher temperature close to 100 °C. The stabilizing effect of the citrate species relies on their immediate adsorption on the particle surface and provides strong electrostatic stabilization, preventing the subsequent aggregation of Ag-NPs. In accordance to Almohammed and Agnihotri,[24,25] the silver nuclei (with size up to 1 nm) appear immediately at the initial moment of irradiation during the photoinduced recovery in an aqueous medium. The nuclei coalesce into particle clusters spontaneously, and further growth of nanostructures occurs as a result of the reduction of silver ions on the surface of the Ag clusters (seed-mediated growth). The mechanism of the silver formation is shown in Fig. 1. Adsorption of the citrate species results in nanoparticle stabilization, greatly minimizing the possibility of aggregate formation. The mechanism of the photoinduced growth of silver particles is associated with the appearance of particles with different charges under the influence of light.[22] The formation of such particles is due to the exchange of electric charges that arise as a result of photoemission through a dispersion medium. This is caused by the dependence of the Fermi energy on the size of the nanoparticles, and leads to equalization of the potential for particles with various sizes. As a result, electric forces arise that contribute to the approach of the particles to a distance at which the van der Waals forces appear, causing aggregation.[26]

The main goal of the present study was focused on the evaluation of how the laser-assisted wet chemical approach towards Ag-NPs affects their spatial parameter-shaping LSPR and their ability to convert energy upon activation *via* 445 nm and 808 nm laser radiation. The temperature effect on the antibacterial properties of modified Ag nanostructures was studied on the *Staphylococcus aureus* population. Based on our previous work,[27,28] we demonstrate the use of the modified Ag-NPs in modern dentistry, namely in endodontics, for nano-laser disinfection of the root canal system of the human tooth.

Experimental

Synthesis of Ag-NPs

Silver nanoparticles were prepared using the laser-assisted wet chemical approach at room temperature (photoinduced recovery of silver ions) by the dissolution of silver nitrate ($AgNO_3$ – 99.8%, Sfera Sim) in distilled water in the presence of trisodium citrate ($Na_3C_6H_5O_7$ – 99.5%, Sfera Sim), which was used as the capping and stabilizing agent. All materials were taken without further purification and treatment. The 445 nm line emitted from a semiconductor continuous wave laser was used for irradiation. Typically, 40 mL of $Na_3C_6H_5O_7$ salt (0.4 mM) was added dropwise into the 10 mL of $AgNO_3$ solution (0.4 mM) under continuous magnetic stirring and 445 nm laser exposure. Upon laser action, the colour of the solution changed from colourless to yellow after 15 min of exposure, pointing out the formation of the spherical Ag-NPs. The process of photoreduction of the Ag^+ ions to Ag^0 by laser radiation was carried out at room temperature (25 °C) for 1 hour.

Modification of Ag-NPs spatial parameters

For the modification of the optical properties of Ag-NPs, we constructed a special device that can be equipped with at least three isolated light sources with different optical characteristics (wavelengths) for simultaneous sample irradiation. The set-up allows for controlling the spatial configuration of silver nanostructures under the influence of the light flux. In our case, two LED strips (LEDs) of 525 nm and 623 nm wavelengths were used as the radiation source in each chamber.

They were located on the inner cylindrical surface of each insulated chamber. Thus, the light was directed uniformly and simultaneously on all sides and the entire height of the chamber. The overall illuminance was 19 000 and 5610 lx, whereas the total radiation power was 148.7 and 177.8 mW for the green and red LEDs, respectively. The set-up construction protected the system from overheating *via* effective cooling, and minimized the occurrence of thermal effects that could affect

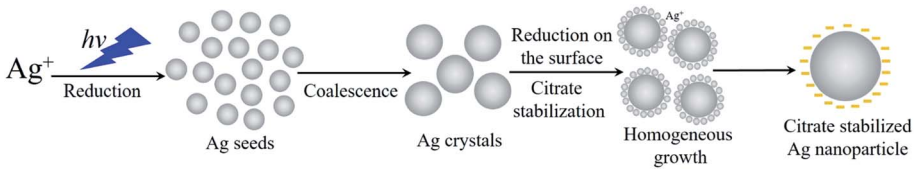

Fig. 1 Scheme of the formation of silver nanoparticles.

the formation and growth of Ag-NPs under laser exposure. The colloidal suspension of Ag-NPs obtained with laser-assisted wet chemical approach was divided into three parts. Each part was placed into a transparent glass vial. The first part was irradiated with red LEDs (FR sample), the second with green LEDs (FG sample), and the last part served as a control in further experiments (F0 sample). The Ag-NPs colloids were left for 6 days with constant exposure at 27 °C.

Physical measurements and apparatus

The particle size and sample morphology of the Ag-NPs were determined by transmission electron microscopy (TEM imaging and site selective area diffraction SAED) using a Tecnai Osiris X-FEG HRTEM transmission electron microscope operating at 200 kV. The standard procedure of sample preparation was used, in which a droplet of diluted Ag-NPs containing colloid was deposited and dried on a 200 mesh copper grid covered with a thin layer of transparent carbon film (EM Resolutions United Kingdom) under dust protection. The mean particle size (d_{av}) was estimated by using image analysis, and calculated with the volume-weighted formula given below:

$$d_{av} = \sum \frac{n_i d_i^4}{n_i d_i^3}, \quad (1)$$

where n_i corresponds to the particle number of a given size and d_i is the diameter of i particle. The concentration of the Ag-NPs in the colloids was determined using a microbalance method utilizing Radwag MYA 5.4Y. This was done by filling up an alumina crucible (of known and stable mass) with 50 μL of the particle dispersion, and allowing for further solvent evaporation until the mass was dry. Three repetitions were done, and the mean mass value was taken for the calculations of concentration.

The absorption spectra of the obtained silver nanostructures were measured on a Cary 5000 UV-VIS-NIR spectrophotometer (Agilent Technologies) using standard cuvettes with an optical path length of 10 mm covering the spectral range from 300 nm (33 333 cm^{-1}) up to 1 μm (10 000 cm^{-1}) using distilled water as a reference.

The hydrodynamic diameter (h.s.) of Ag-NPs was estimated by dynamic light scattering (backscatter laser radiation at the angle of 173°) technique, together with particle distribution (polydispersity index, PdI). The optimal concentration was found to be 60 μg mL^{-1}, assuring repeatable and reliable results. For this experiment, a universal Nanoplus HD 3 set-up (Particulate System/Micrometrics) equipped with a 660 nm laser diode was used, and the obtained data were analyzed with dedicated software provided by the set-up manufacturer.

The heat generation experiments were conducted by using two laser sources: 445 nm continuous laser diode with TTL modulation (Eshine, China) and controlled power (maximum output power is 1 W, beam divergence < 3 mrad) and 880 nm continuous semiconducting laser (CNI, China) with controlled laser power (1.8 W maximum output power after the fiber, laser power stability below 1%) was used. Prior to measurements, calibration of the laser sources was made with an Ophir StarLite laser power meter equipped with a beam track thermal sensor 10 A-PPS (measurable laser powers from 20 mW up to 10 W, laser beam size detection with 5% accuracy – Ophir, Israel). The samples were protected with a self-made black box to limit heat exchange with the environment. In order to monitor the sample temperature changes, a FLIR T660 thermovision camera was used. Obtained data were analyzed with ResearchIR dedicated software provided by FLIR. The exact same set-up configuration was used to monitor the temperature effects of the Ag-NPs colloids administrated directly into the teeth channel.

Six human mandibular premolar teeth, which were extracted for orthodontic purposes, were used. The teeth preparation was carried out in the Department of Therapeutic Dentistry, Lviv National Medical University after the approval by the ethical committee of the University.

Antibacterial activity of Ag nanostructures

Gram-positive bacteria strain, *Staphylococcus aureus* (ATCC 25923), from the microbial collection of the University of Rzeszow, Poland, was employed to evaluate the potential of antibacterial activity of the silver nanostructures. Nutrient broth (NB) or agar (NA) was used for the preparation of the bacterial culture suspension. For serial dilutions, phosphate buffered saline (1× PBS; 137 mM NaCl, 2.7 mM KCl, 10 mM Na_2HPO_4, 1.8 mM KH_2PO_4) was used. All media were purchased from BTL company (Poland) and Sigma-Aldrich (USA). The inoculum, performed using suspended 50 μL of bacteria strain with 5 mL of NB, was precultivated for 24 h at 37 °C on a rotatory shaker (150 rpm). The reduction in the number of bacteria cells after nanostructure exposure was evaluated as described before,[29] with some modifications. Briefly, the bacteria preculture was mixed with each of the tested solutions of nanostructures (F0, FG, and FR with the initial concentration of 0.4 mg mL^{-1}), in a ratio of 1 : 1, followed by irradiating (3 min) with a blue (445 nm and optical density of 0.28 W cm^{-2}) and red (880 nm and optical density of 0.28 W cm^{-2}) laser beam for the F0 and FR or FG and FR nanostructure samples, respectively. To

simplify the sample nomenclature in this study, a system of abbreviations was used (*e.g.*, $F0_{blue}$ stands for the F0 sample irradiated with a blue laser beam). To avoid the impact of the light, the samples were then covered by foil and incubated for 2 additional hours at 37 °C. The sampling time for this experiment was 2 h. Afterwards, these aliquots were taken, serially diluted, and plated onto the agar plates. The control experiments were performed identically, albeit without exposure to the laser irradiation. After 24 h of incubation, bacteria colony forming unions (CFU) were counted and the percentage of reduction (%*R*) in the growth was estimated, according to the formula:

$$\%R = \left(\frac{\text{CFU control} - \text{CFU sample}}{\text{CFU control}}\right) \times 100\% \qquad (2)$$

The test was done in duplicate, and the mean and standard deviation were estimated.

Results and discussion

Silver nanoparticles characterization

The particle size and morphology of the Ag-NPs fabricated through the laser-assisted wet chemical approach were evaluated through analysis of the TEM images (Fig. 2). As one can note, the sample denoted as F0 (Fig. 2(a)) contained predominantly spherical metallic silver particles with a mean size of 48 nm (±7 nm). The inset in Fig. 2(a) shows the results of the selected area electron diffraction (SAED) pattern of the Ag NPs. Prolonged irradiation of the Ag-NPs stock with the green LEDs (525 nm) resulted in a partial morphology transformation into triangular nanoparticles (Fig. 2(b)), accompanied by the growth process that led to the formation of 98 nm (±17 nm) Ag-NPs (hereafter sample FG). The same exposure time (6 days) of the F0 colloid sample under the constant action of the red LEDs (623 nm) favored the growth of the silver nanotriangles with a mean length close to 155 nm. Jing An[30] explored the mechanism of the effect of light on the conversion and growth of Ag nanoparticles, and showed that prolonged expositing of triangular nanoprisms led to the formation of hexagonal nanoplates. Thus, the FR sample contained a significant number of particles with other types of morphologies as well (see Fig. 2(c)). The difference in the obtained Ag-NPs is also reflected in the color of the resulting suspensions (Fig. 2 vial insets), changing from yellow (spherical geometry) to blue (triangular shapes) and finally to green, suggesting variance in the spectral behaviour, *i.e.*, absorption spectra.

The hydrodynamic size (h.s.) was measured in order to provide data on the agglomeration state of Ag-NPs, as well as the colloidal stability of the fabricated NPs dispersion at neutral pH. This factor is of great importance in bioapplications determining material applicability and predictability of physicochemical properties. The hydrodynamic size of Ag-NPs for the F0 sample was 50 nm (polydispersity index PdI – 0.22), FG 85 nm (PdI – 0.3). For the FR NPs, the hydrodynamic size was around 90 nm (PdI – 0.26). It can be concluded that the NPs diameters in the solution correspond well with the TEM data with an exception existing for the FR sample. This is caused by the model used for the fitting results, which assumes that the particle shape is spherical. Thus, in this case, there are some parts of the nanorod morphology that will not lead to the perfect match between the calculations based on a used algorithm and the experimental results. The values of the PdI are characteristic for the rather polydisperse colloids, but with a small aggregation degree. It seems that the laser-assisted wet chemical approach towards Ag-NPs can be sought as a convenient protocol for the morphology control of the particles due to its simplicity. However, it will need further improvements to give a product with slightly better characteristics. There are many well-known alternative ways to control the nanoparticles morphology during synthesis. For instance, Jing An[30] used a high-power source (70 W sodium lamp) for the growth process of the hexagonal silver nanoplates. Huang and Kim[31] grew Au nanoparticle seeds by photoresponsive surfactant under the dangerous (for human) UV irradiation (365 nm). Pastoriza-Santos[32] described the growth process of Ag nanoprisms by

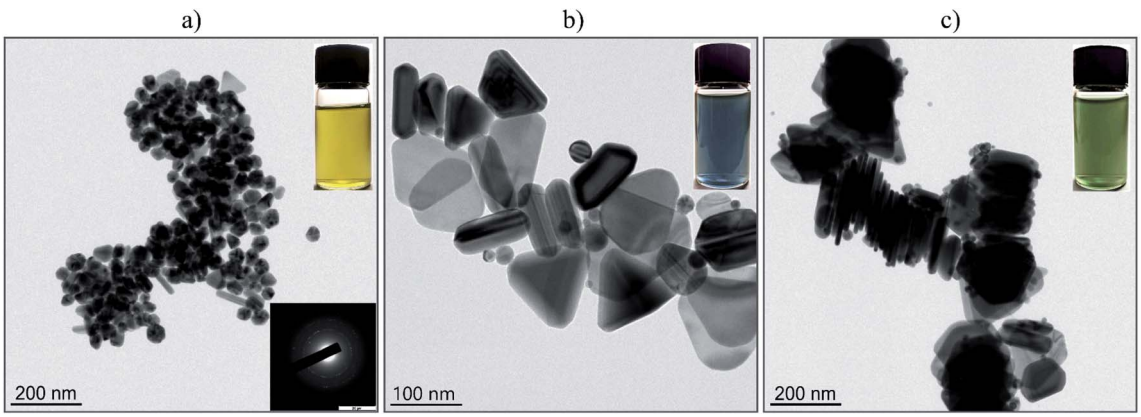

Fig. 2 TEM images of the stock Ag-NPs colloids (a) with SAED pattern of Ag NPs (inset), Ag-NPs (FG) after green LEDs (525 nm) action (b) as well as Ag-NPs (FR) exposed to red LEDs (623 nm) (c). Insets in the images show the colour variation of the Ag-NPs suspensions depending on the spatial geometry changes.

boiling $AgNO_3$. Compared to these methods, we used safe visible light sources up to 400 mW and our method does not require boiling.

Optical properties of Ag nanoparticles and theoretical calculations

The absorption spectra of silver colloids were recorded in order to evaluate and compare their optical properties (Fig. 3). The F0 sample shows a typical absorption peak (Fig. 2(a)) with a maximum located at 423 nm associated with the surface plasmon resonance position of the spherical Ag-NPs.[33] The change in the sample morphology induced with the green LEDs (FG) was clearly evidenced by the absorption spectra. Still, a 420 nm plasmon band is present. However, the two additional peaks can be individuated, one at around 630 nm and the second is shifted towards the red spectral range with a maxima at 866 nm (Fig. 3(b)).

What is interesting is that irradiation of the FR sample with 623 nm LEDs during synthesis resulted in diminishing the peak around 630 nm, and enhancement of the relative absorption of the NIR spectral range (shoulder at 680 nm and maximum at 934 nm). Moreover, the intensity of the 420 nm band decreased upon synthetic conditions, reflecting the changes in the total fraction of spherical Ag-NPs in FG and FR colloids. The appearance of the peak at the NIR region is of particular value. It gives direct evidence of the changes in the spatial geometry of Ag-NPs. In addition, it can be used further in biological applications, *i.e.*, photo or photothermal therapy since it covers the Ist biological optical window.[34] Moreover, the intensity of the additional peaks is stronger than the initial 423 nm peak. It can be assumed that this is due to the localized surface plasmon resonance, which occurs under the influence of the incident wave. This wave creates a temporary dipole, causing the attachment of free silver ions in the solution to the formed nanospheres.[35] Thus, modification of the spatial Ag-NPs geometry and particle size directly results in a shift of the plasmon peak positions, and a change of the optical properties of metallic nanoparticles.

The nature of those two additional peaks revealed in the absorption spectra of the FG and FR samples can be associated with the optical behavior of triangular nanostructures, which are usually characterized by double localized plasmon resonance peaks with the meaningful difference in the intensity of the individual LSPR peaks.[36,37]

In order to gain deeper insight into the experimental data, theoretical simulations on the LSPR peak positions for all Ag-NPs samples were performed using the freely available DDSCAT+ software[38] based on the discrete dipole approximation (DDA) method. The DDA approach can be exploited for modelling the optical properties of arbitrary morphology nanostructures in comparison to the commonly used approach for exploring the light behavior based on Maxwell's theory,[12] which is used for nano-objects with limited simple geometries. DDA discretizes objects into a set of dipoles (polarizable points). In this sense, the interaction of light with each polarizable point can be calculated separately. Thus, the quantitative characteristic calculated using DDSCAT+ is a light absorption efficiency factor Q_{abs} defined as follows:

$$Q_{abs} = \frac{C_{abs}}{\pi(3V/4\pi)^{\frac{2}{3}}}, \quad (3)$$

where C_{abs} is the absorption cross section, and V stands for the nano-object's volume. For the fitting purpose of the F0 colloid, a nanoparticle diameter of 50 nm and the medium refractive index of 1.33 were taken. The results of the theoretical calculations show a very good agreement with the experimental data (Fig. 3). Therefore, it can be concluded that the optical properties of the F0 sample are predominantly governed by the plasmonic effect on spherical Ag particles. As far as the FG suspension is concerned, the situation is a bit more complex since the absorption spectra contain more peaks. Thus, three nanotriangle dimensions (taking into account their edge length) have been used: 85 nm (most abundant), 175 nm (some fraction), and 350 nm (few objects) basing on the TEM analysis. It was found that the thickness of the nanotriangles decreases with increasing edge lengths. This conclusion correlates well

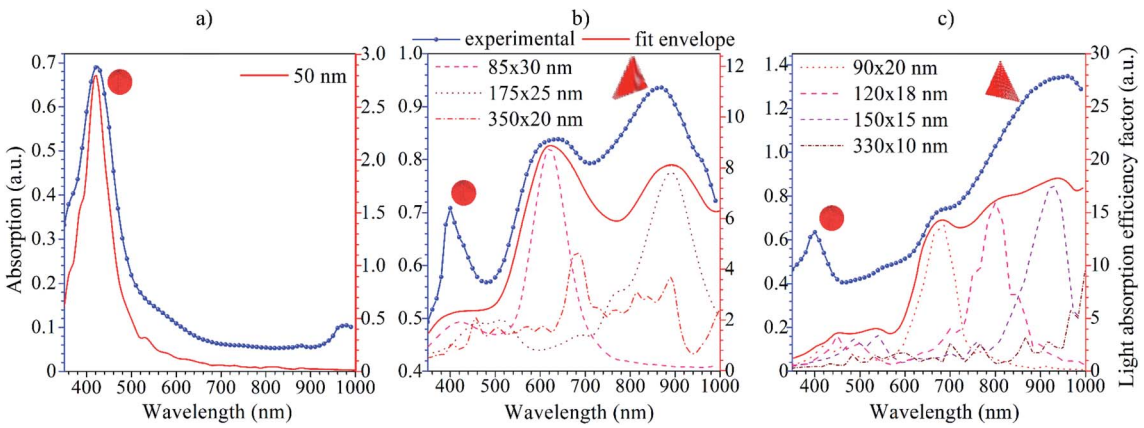

Fig. 3 Absorption spectra of the F0 (a), FG (b) and FR (c) Ag-NPs colloidal suspensions with the results of theoretical modelling using the DDA approach.

with the TEM image (Fig. 2(b)). Therefore, theoretical modelling allows one to estimate the thickness of the triangular nanostructures. Based on the set of numerical calculations, it was supposed that the thicknesses of the nanotriangles with the following edge lengths, 85, 175 and 350 nm, were 30, 25 and 20 nm, respectively. As one can see, the 85 × 30 nm triangular NPs should have an intense absorption peak at 620 nm, whereas the 175 × 20 nm triangles will have a maximum absorption peak located at 890 nm, which is exactly the case (compared with experimental data). The contribution of the 350 × 20 nm objects to the absorption spectra of the FG sample will be of influence. Superposition of both absorption spectra for the 85 × 30 nm and 175 × 20 nm triangular particles corresponds to the recorded data very well. The resulting fit envelope curve is characterized by two maximum values, corresponding to the LSPR peaks position on the experimental curve. The mismatch between the mutual intensity relationship of the peaks is related to the definite NPs fraction with different spatial geometries of the specific colloid. The peak at around 420 nm points out the presence of some content of spherical Ag-NPs, as well as leaving some space for synthetic protocol optimization or allows for the preparation of broadly absorbing materials. In the case of the FR sample containing the largest objects and interesting morphology changes for the fitting model, the particle diameters of 90, 120, 150 and 330 nm were used (Fig. 3(c)). It should be noted that the FR sample shows the same pattern as established for the FG sample. The nanotriangle thickness decreases with an increase of edge length. For the given object sizes of 90, 120, 150 and 330 nm, the thickness is 20, 18, 15 and 10 nm, respectively. It can be seen that the peak associated with large particles (330 × 10 nm) is shifted towards the IR range. The theoretical curve obtained in the simulation of the FR spectral behaviour corresponds well with the experimental one (Fig. 3(c)). The fit was also performed for the Ag nanorods since the TEM image (Fig. 2(c)) may suggest the presence of this particular morphology instead, which is believed to be tilted triangles exposing only the edges. In the case of the nanorods with the assumed 150 × 15 nm size, the fitted absorption spectra is characterized by the anticipated peak at 350 nm, whereas the triangles of the same diameter give the peak with the maximum located at 950 nm. The same observation was reported by Kelly[39] and Lesyuk.[40] In conclusion, by adopting this synthetic protocol, one can fabricate the Ag-NP with different plasmonic properties covering the spectral range from UV to NIR that opens several interesting possibilities for biological applications.

Energy conversion of Ag nanostructures

The temperature effects of the F0, FG and FR Ag-NPs colloids were measured using 445 and 880 nm lasers as a function of the optical laser density and nanoparticle concentration (Fig. 4–6). In order to limit the sample exposure to the laser radiation, the duration of each experiment did not exceed 10 minutes and the OD maximum value was not higher than 0.28 W cm^{-2}. It was slightly below the safety limit of 0.33 W cm^{-2} for the biological systems.[34] The choice of the specific wavelengths was based on a match with the absorption bands of the Ag-NPs plasmonic resonance peaks. Under such conditions, the maximum light absorption was achieved for each tested colloids. The heat induction was measured using 0.5 mL of the respective Ag-NPs suspensions with defined concentration.

In the case of the F0 sample, the 445 nm laser was used, exclusively, to induce heating since only one plasmonic peak appeared in the spectra with the position correlating with the chosen 445 nm light source (see Fig. 3(a)). As one can see, an increase of the laser OD and F0 Ag-NPs concentration (Fig. 4) greatly enhanced the colloid heating ability, with an almost 10-fold change between 0.07 and 0.28 W cm^{-2} observed for the 1 mg mL^{-1} concentration. The maximum ΔT was achieved for the F0 spherical particles with the concentration above 0.8 mg mL^{-1} and 0.28 W cm^{-2}. A decrease of the Ag-NPs concentration results in a lower maximum temperature that can be achieved due to the decreasing number of nanoheaters within the constant medium volume.

The heating ability of the FG sample, which shows two distinct absorption peaks (Fig. 3(b)), was measured using the following wavelengths, 445 nm and 880 nm, in order to compare the effectiveness of the energy conversion under stimulation at different spectral regimes (Fig. 5). As we evidenced before, the FG sample contains two morphologically distinct Ag-NPs, a fraction of spheres and triangles. In fact, the maximum ΔT (55 °C) was achieved for the 880 nm stimulation with the highest OD (0.28 W cm^{-2}), whereas the 445 nm laser irradiation resulted in a temperature change below 10 °C for the same OD and the same concentration of nanoparticles (1 mg mL^{-1}). This is due to the LSPR peak intensity difference and absorption cross section, as indicated in Fig. 3(b).

Analysis of the FR Ag-NPs temperature behaviour (Fig. 6) shows that the relative temperature ΔT (maximum value is around 12 °C) upon irradiation with 445 nm depends strongly on the optical power density and NPs concentration.

At a low OD regime (0.07 W cm^{-2}), the ΔT for the blue laser was only 1.7 °C, being within temperature error. However, action of the 880 nm light results in ΔT that is quite comparable with the FG colloid suspensions. Thus, it may be concluded that the FR and FG colloid heating is very efficient under NIR exposure due to the similarities in the optical behaviour.

The specific absorption rate (SAR) was calculated for all Ag-NPs colloids to estimate and compare the efficacy of the energy conversion using the following equation:

$$\mathrm{SAR} = \frac{C}{m}\frac{\partial T}{\partial t}, \tag{4}$$

where C depicts the specific heat capacity of the suspending medium (C_{H_2O} – 4185 J dm^{-3} K^{-1}), m stands for the Ag-NPs concentration in a given dispersion (g dm^{-3}), and dT/dt is the slope of the heating curve fitted with a linear model for the very first seconds of the temperature evolution.[41] In the literature, SAR is a widely accepted measure of the material heating ability. Results of the calculations are gathered in Table 1. For quick comparison, we considered colloids with the concentration of 1 mg mL^{-1} Ag nanoparticles.

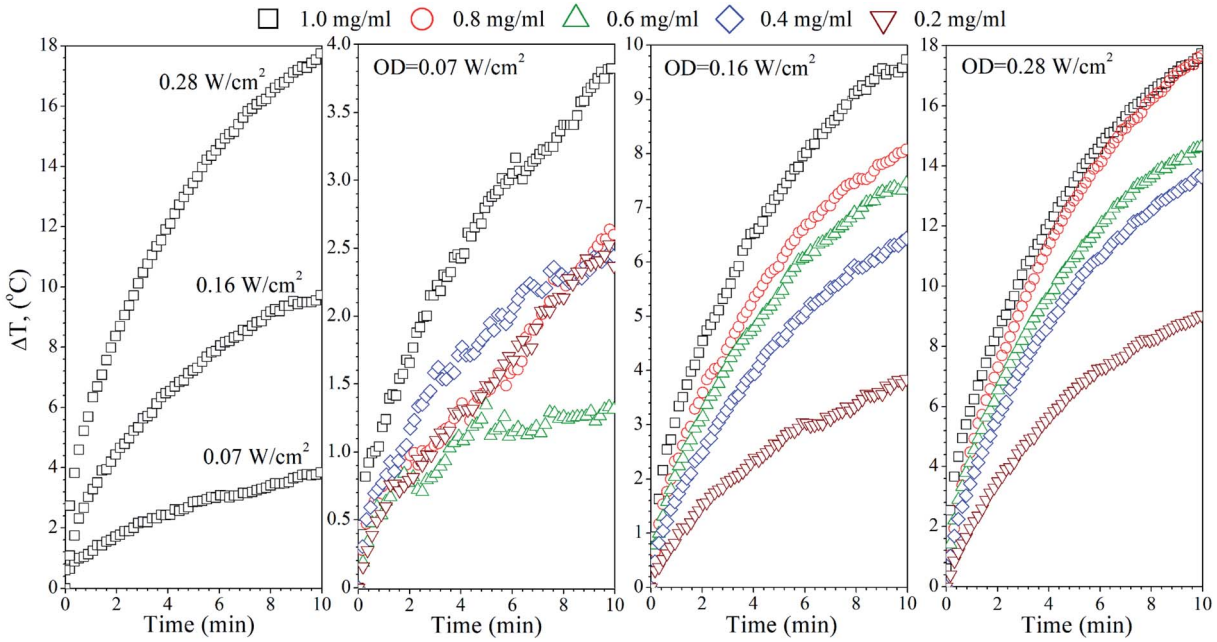

Fig. 4 Temperature dependence of the Ag-NPs colloid (F0 – 1 mg mL^{-1}) as a function of the optical density (left plot) and concentration effect of the Ag-NPs on the heating ability under exposure to 445 nm laser at different ODs: 0.07, 0.16 and 0.28 W cm^{-2}.

What is worth noting is that the SAR values for the F0, FG and FR samples under 445 nm vary, but these differences are directly reflected in the LSPR intensities. For instance, at 0.28 W cm^{-2}, SAR_{F0} is 320 W g^{-1}, SAR_{FG} 126 W g^{-1} and SAR_{FR} 182 W g^{-1}, respectively. Moreover, at OD 0.07 W cm^{-2}, the FG and FR samples did not show a meaningful temperature increase. The situation completely changes upon NIR exposure. It can be seen that for the same laser power densities, the specific absorption rates for the 445 nm and 880 nm wavelengths are very different. Since the F0 colloid has no absorption peak in the NIR range, it does not respond to the 880 nm laser stimulation, whereas the FG and FR suspensions show the high intensity and broad

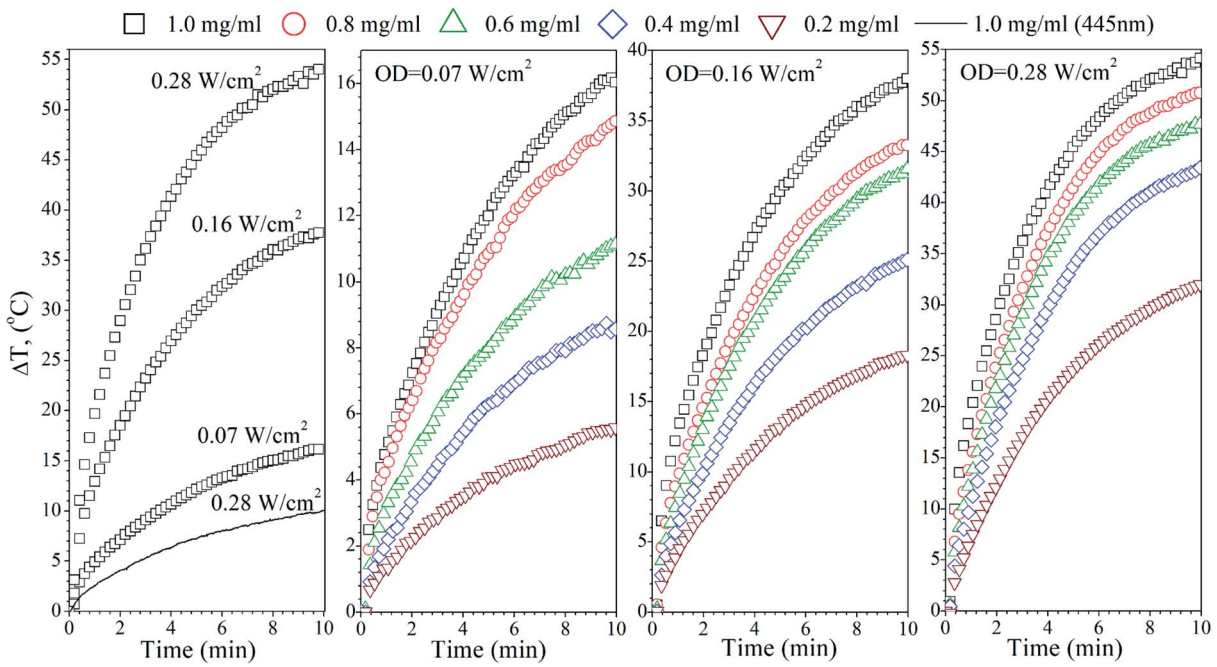

Fig. 5 Temperature dependence of the Ag-NPs colloid (FG – 1 mg mL^{-1}) as a function of the optical density (left plot) and concentration effect of the Ag-NPs on heating ability under exposure of 880 nm laser at different ODs: 0.07, 0.16 and 0.28 W cm^{-2}. The black line shows the temperature increase upon the action of 445 nm for comparison (left plot).

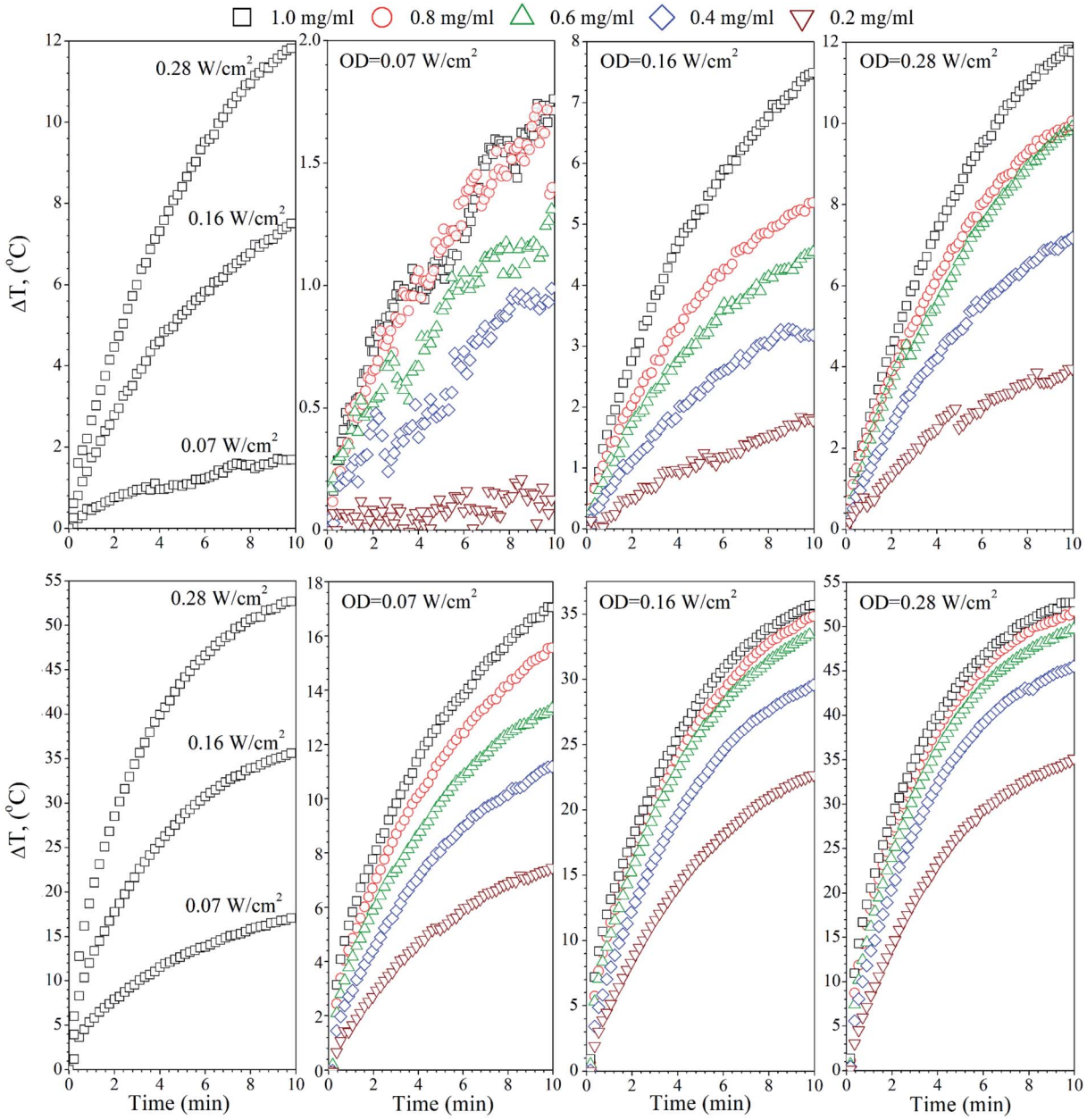

Fig. 6 Temperature dependence of the Ag-NPs colloid (FR – 1 mg mL^{-1}) as a function of the optical density (left plot) and concentration effect of the Ag-NPs on heating ability under exposure to 445 nm (top panel) and 880 nm (bottom panel) lasers at different ODs: 0.07, 0.16 and 0.28 W cm^{-2}.

plasmonic bands. The SAR for the FG and FR depends naturally on the applied OD, and changes in a comparable manner in both cases from the 490 W g^{-1} at an OD value of 0.07 W cm^{-2} up to the extremely high SAR value exceeding 1500 W g^{-1} upon 0.28 W cm^{-2}. The presented data clearly points out on the fact that the non-spherical Ag-NPs with modified optical properties allow for achieving a higher temperature effect at the same exposure time, optical density and NPs concentration in comparison with the spherical nanostructures. For instance, the SAR value near 0.6 kW g^{-1} was observed by Bandarra Filho[42] for different concentrations of spherical silver nanofluids under the direct sunlight. These values are higher than for many magnetic nanoparticles under the strong magnetic fields (normally below 0.3 kW g^{-1}) for applications in hyperthermia. Thus, such high efficiency of the energy conversion connected with the ability of nanostructures to absorb radiation in the NIR spectral region is very important for the practical application in bio-related fields.

The practical application prospect of Ag-NPs colloids in dentistry for the rapid disinfection of the tooth canals and cavities was tested. The tooth root canal was filled with the FR nanoparticle suspension with 0.4 mg mL^{-1} concentration, taking a small droplet (15 μL) of colloid (6 μg of Ag-NPs). The dental canal was dried with a laboratory dryer, and the tooth

Table 1 Specific absorption rate (SAR) and dT/dt values of the Ag-NPs colloids under stimulation of 445 and 880 nm laser sources with different optical laser densities (OD)

Sample	Wavelength (nm)	OD (W cm^{-2})	dT/dt (°C s^{-1})	SAR (W g^{-1})
F0	445	0.07	0.03	61.48
		0.16	0.08	158.72
		0.28	0.15	320.32
FG	445	0.28	0.06	126.89
	880	0.07	0.23	490.36
		0.16	0.44	927.298
		0.28	0.72	1500.97
FR	445	0.07	0.01	20.76
		0.16	0.03	62.59
		0.28	0.09	182.72
	880	0.07	0.24	496.57
		0.16	0.60	1255.04
		0.28	0.73	1522.42

was placed in the experimental set-up. Afterward, it was irradiated with the 445 and 880 nm laser lights for 10 minutes. As one can see (Fig. 7), the 445 nm exposure of the tooth with and without Ag-NPs caused a similar temperature increase, pointing out that there is no added value due to the usage of this particular wavelength.

The temperature increase of the tooth without particles is due to the self-absorption of a bone tooth, which constitutes calcium apatite (calcium hydroxyapatite, tricalcium phosphate, *etc.*). In constrast, NIR stimulation leads to a higher temperature increase. The ΔT in this case is around 20 °C with particles and 15 °C for the control tooth, respectively. It is expected that the further increase of the Ag-NPs concentration will lead to more spectacular temperature effects, allowing for a shorter duration of light exposure. Therefore, it is anticipated that the application of such Ag-NPs under laser stimulation might assure better results in terms of disinfection of the tooth during dental treatment, benefiting also from the antibacterial properties of the Ag-NPs.

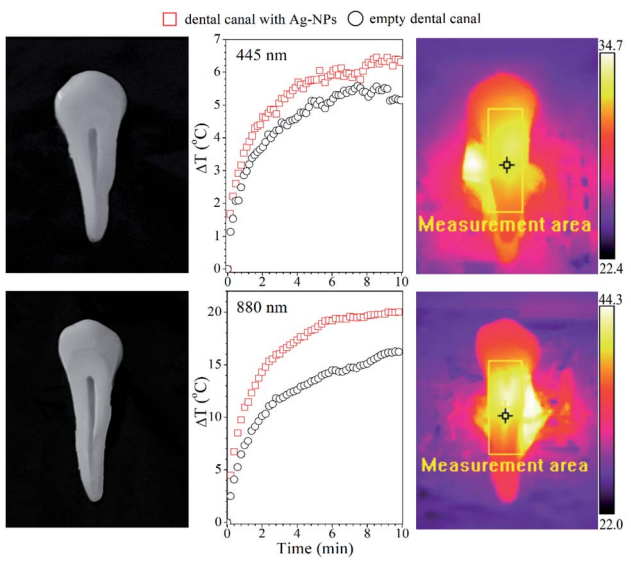

Fig. 7 Temperature changes in the dental canal with and without FR Ag-NPs (6 μg) during irradiation with a wavelength of 445 nm (top panel) and 880 nm (bottom panel).

Antibacterial effect of the Ag-NPs

The next point of this work was to study the impact of the blue and red light-modified silver nanostructures on *Staphylococcus aureus*. The phenomenon of the antimicrobial activity of the silver ions and nanoparticles has been well studied, and was reported in our previous data.[43–45]

Moreover, the impact of the nanostructure component of the F0, FG and FR samples on the microbial strains has been checked, and their toxicities were noted (data not shown). However, the main aim of this assay was to assess the antibacterial effect of the modified nanoparticles (F0, FG and FR samples) after additional exposure of each sample to a laser beam, regarding their bioapplication possibility. Accordingly, the experiment was conducted to check whether the heat generation by the nanostructures after irradiation has an impact on the bacterial cell population. The practical application of this procedure could be the use of nanoparticles as an additive to dental plaque. Thanks to the exposure of the dental plaque doped with nanoparticles (*e.g.*, UV or red light used in dentistry), it would be possible to obtain an additional septic effect and a lasting bactericidal effect in the treated teeth.

The choice of the type of light was dependent on the previous results, where the UV-Vis absorption spectra were determined and the appearance of additional peaks in the blue and near-infrared region of wavelengths were recorded (Fig. 3). Red and blue light were used to irradiate the FG and FR samples or F0 and FR samples, respectively. All measurements were also performed for the sample with the concentration of 0.4 mg mL^{-1}. Fig. 8 shows the percentage reduction of the bacteria cell population after exposure to the various irradiated nanostructures. For sample FG and FR after red laser irradiation, the higher impact on the inhibition of *Staphylococcus aureus* was noticed,

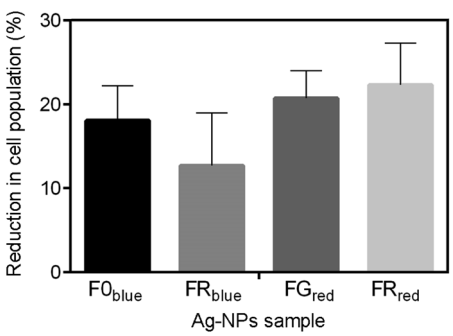

Fig. 8 The percentage reduction in the cell population of *Staphylococcus aureus* ATCC 25923 exposed to modified silver nanostructure after 3 min of exposure to blue or red light and 2 h recovery. Data are expressed as the mean of duplicates ± standard deviation. The bar graphs show no significance according to the Tukey's multiple comparisons test.

and was equal to 21 and 22% of the cell population reduction, respectively.

A slightly lower reduction was observed for bacterial exposure to the F0 and FR samples irradiated with a blue laser, which was equal to 18 and 13% reduction in the number of cells. Although, the decrease in population of the bacteria was noticed in all cases, the percentage of the reduction could be higher when the various concentrations and time of exposure would have been implemented.

Indeed, Cheon *et al.*[46] reported on the antibacterial activity of silver nanostructures, which was improved as the concentration of the NPs increased from 0.1 to 0.7 mg mL^{-1}. Moreover, the authors also proved that the antimicrobial efficacy of silver NPs depends on their shape and size. Spherical nanoparticles were found to be more effective in delaying the growth of *E. coli* than nanoparticles of disk-like shape, while the triangular shaped nanoparticles exhibited the strongest antimicrobial properties.[46] The difference in the antibacterial activity noted for tested samples may be interpreted from the point of view of the surface area,[47] which stays in contact with the bacterial cells and effluent. Thus, the nanoparticle size and morphology may strongly affect the reduction rate in the cell population.

Conclusions

Silver nanoparticles with a predominantly spherical shape and mean size of 48 nm (±7 nm) with a plasmonic peak at 423 nm were synthesized through the laser-assisted wet chemical approach at the room temperature. The morphology and optical parameters of the Ag NPs were modified with green (525 nm) and red (623 nm) LEDs.

It has been shown that the prolonged irradiation of Ag colloids by LEDs leads to the appearance of additional plasmon absorption peaks at the NIR spectral region, 866 and 934 nm, respectively. The numerical calculations of the LSPR peak positions for all Ag-NPs samples were carried out by the discrete dipole approximation method. The results of the simulation revealed that 175 × 20 nm and 150 × 15 nm triangles are responsible for the appearance of the plasmon absorption peaks at the NIR region.

The energy conversion of the Ag nanostructures was evaluated. It has been found that the light-modified Ag-NPs demonstrated the most efficient conversion of light energy into heat under exposure to the NIR irradiation. Increase of the Ag NPs concentration and laser power density resulted in faster heating. SAR calculations have shown high efficiency of the energy conversion, and thus the potential for biological applications.

Applicability of the light-modified Ag-NPs in dentistry for the rapid disinfection of the tooth canals and cavities was tested. It was shown that the synergic effect of the Ag-NPs heating and antibacterial properties can be beneficially utilized in dentistry. The impact of the light-modified Ag NPs on *Staphylococcus aureus* was defined as well. We have shown that irradiation of the silver nanostructures with a concentration of 0.4 mg mL^{-1} for 3 min leads to a reduction of the bacteria population of about 20%. It was assumed that the effect could be significantly enhanced by either an increase of the nanoparticle concentration or extension of the exposure time.

Conflicts of interest

There are no conflicts to declare.

Acknowledgements

The authors would like to acknowledge the following funding agencies for support: National Science Centre project no. UMO-2017/25/B/ST5/00497 (R. P.), Polish National Agency for Academic Exchange (NAWA) within Prom program (T. B.), as well as the Ministry of Education and Science of Ukraine, grant DB/Interface no. 0120u100675 (T. B., I. Ya.). T. B. would like to thank Andrzej Dziedzic for the TEM characterization and Daniel Sikora (biotechnology student at UR) for his assistance in conducting measurements.

References

1 C. Burda, X. Chen, *et al.*, Chemistry and properties of nanocrystals of different shapes, *Chem. Rev.*, 2005, **105**(4), 1025–1102.
2 H. Chugh, D. Sood, I. Chandra, V. Tomar, G. Dhawan and R. Chandra, Role of gold and silver nanoparticles in cancer nano-medicine, *Artif. Cells, Nanomed., Biotechnol.*, 2018, **46**, 1210–1220.
3 C. Loo, A. Lowery, N. Halas, J. West and R. Drezek, Immunotargeted nanoshells for integrated cancer imaging and therapy, *Nano Lett.*, 2005, **5**(4), 709–711.
4 X. F. Zhang, Z. G. Liu, W. Shen and S. Gurunathan, Silver nanoparticles: synthesis, characterization, properties, applications, and therapeutic approaches, *Int. J. Mol. Sci.*, 2016, **17**(9), 1534.
5 E. Abbasi, M. Milani, S. Fekri Aval, M. Kouhi, A. Akbarzadeh, H. Tayefi Nasrabadi and M. Samiei, Silver nanoparticles: synthesis methods, bio-applications and properties, *Crit. Rev. Microbiol.*, 2016, **42**(2), 173–180.
6 M. Murphy, K. Ting, X. Zhang, C. Soo and Z. Zheng, Current development of silver nanoparticle preparation, investigation, and application in the field of medicine, *J. Nanomater.*, 2015, 1–12.
7 J. S. Kim, *et al.*, Antimicrobial effects of silver nanoparticles, *Nanomedicine*, 2007, **3**(1), 95–101.
8 H. Liao, C. L. Nehl and J. H. Hafner, Biomedical applications of plasmon resonant metal nanoparticles, *Nanomedicine*, 2006, **1**(2), 201–208.
9 J. Z. Zhang and C. Noguez, Plasmonic optical properties and applications of metal nanostructures, *Plasmonics*, 2008, **3**(4), 127–150.
10 S. Bhakya, S. Muthukrishnan, M. Sukumaran and M. Muthukumar, Biogenic synthesis of silver nanoparticles and their antioxidant and antibacterial activity, *Appl. Nanosci.*, 2016, **6**(5), 755–766.

11 J. Zhao, X. Zhang, C. R. Yonzon, A. J. Haes and R. P. Van Duyne, Localized surface plasmon resonance biosensors, *Nanomedicine*, 2006, **1**(2), 219–228.

12 S. Maier, *Plasmonics: fundamentals and applications*, Springer, New York, 2007.

13 A. Amirjani, N. N. Koochak and D. F. Haghshenas, Investigating the Shape and Size-Dependent Optical Properties of Silver Nanostructures Using UV–vis Spectroscopy, *J. Chem. Educ.*, 2019, **96**(11), 2584–2589.

14 N. G. Khlebtsov, Optics and biophotonics of nanoparticles with plasmon resonance, *Quantum Electron.*, 2008, **38**(6), 504–529.

15 T. Bulavinets, V. Varyshchuk, I. Yaremchuk and Y. Bobitski, Design and Synthesis of Silver Nanoparticles with Different Shapes under the Influence of Photon Flows, in *Nanooptics, Nanophotonics, Nanostructures, and Their Applications*, ed. O. Fesenko and L. Yatsenko, 2018, vol. 210, pp. 231–241.

16 K. L. Kelly, E. Coronado, L. L. Zhao and G. C. Schatz, The optical properties of metal nanoparticles: the influence of size, shape, and dielectric environment, *J. Phys. Chem. B*, 2003, **107**, 668–677.

17 J. Z. Zhang, Biomedical applications of shape-controlled plasmonic nanostructures: a case study of hollow gold nanospheres for photothermal ablation therapy of cancer, *J. Phys. Chem. Lett.*, 2010, **1**(4), 686–695.

18 S. M. Razavinia, M. H. Nazarpak, F. Fayyazbakhsh, Z. Aminipour, A. Keshtkar and M. Solati-Hashjin, Synthesis of Triangular Silver Nanoprisms: The Role of Reagents on Shape-Dependent Antibacterial Properties for Dental Applications, *Artif. Organs*, 2013, **37**(7), 48.

19 R. Y. Sato-Berrú, A. R. Vázquez-Olmos, E. V. Mejía-Uriarte, M. E. Mata-Zamora, A. Solís-Gómez, F. Paraguay-Delgado and J. M. Saniger, Synthesis of Silver Colloids with a Homemade Light Source, *J. Cluster Sci.*, 2018, **29**(4), 719–724.

20 J. Krajczewski, K. Kołątaj and A. Kudelski, Light-induced growth of various silver seed nanoparticles: a simple method of synthesis of different silver colloidal SERS substrates, *Chem. Phys. Lett.*, 2015, **625**, 84–90.

21 D. G. Cahill, W. K. Ford, K. E. Goodson, G. D. Mahan, A. Majumdar, H. J. Maris and S. R. Phillpot, Nanoscale thermal transport, *J. Appl. Phys.*, 2003, **93**(2), 793–818.

22 Z. I. Bespalova and A. V. Khramenkova, The use of transient electrolysis in the technology of oxide composite nanostructured materials, *Nanosyst.: Phys., Chem., Math.*, 2016, **7**(3), 433.

23 X. Dong, X. Ji, H. Wu, L. Zhao, J. Li and W. Yang, Shape control of silver nanoparticles by stepwise citrate reduction, *J. Phys. Chem. C*, 2009, **113**(16), 6573–6576.

24 S. Almohammed, F. Zhang, B. J. Rodriguez and J. H. Rice, Photo-induced surface-enhanced Raman spectroscopy from a diphenylalanine peptide nanotube-metal nanoparticle template, *Sci. Rep.*, 2018, **8**(1), 3880.

25 S. Agnihotri, S. Mukherji and S. Mukherji, Size-controlled silver nanoparticles synthesized over the range 5–100 nm using the same protocol and their antibacterial efficacy, *RSC Adv.*, 2014, **4**(8), 3974–3983.

26 P. K. Khanna, N. Singh, S. Charan, V. V. V. S. Subbarao, R. Gokhale and U. P. Mulik, Synthesis and characterization of Ag/PVA nanocomposite by chemical reduction method, *Mater. Chem. Phys.*, 2005, **93**(1), 117–121.

27 A. Ya. Barylyak, Nanolaser disinfection of the tooth root canal system, *Reports of the National Academy of Sciences of Ukraine*, 2008, **9**, 180–183.

28 A. Barylyak, Ya. Bobitski, J. Vernish, A. Georgopolos, O. Zaichenko, V. Zubachyk, O. Zubachyk, A. Moritz, O. Shevchuk and U. Shup vynakhidnyky, Lviv Polytechnic National University and Lviv National Medical University named after D. Halytsky, patentovlasnyky, Sposib dezinfekcii korenevoho kanaly zyba, Patent Ukrainy no. 25845, 2007, Ser. 27.

29 M. Parlinska-Wojtan, M. Kus-Liskiewicz, J. Depciuch and O. Sadik, Green synthesis and antibacterial effects of aqueous colloidal solutions of silver nanoparticles using camomile terpenoids as a combined reducing and capping agent, *Bioprocess Biosyst. Eng.*, 2016, **39**(8), 1213–1223.

30 J. An, B. Tang, X. Ning, J. Zhou, S. Xu, B. Zhao and J. R. Lombardi, Photoinduced shape evolution: from triangular to hexagonal silver nanoplates, *J. Phys. Chem. C*, 2007, **111**(49), 18055–18059.

31 Y. Huang and D. H. Kim, Light-controlled synthesis of gold nanoparticles using a rigid, photoresponsive surfactant, *Nanoscale*, 2012, **4**(20), 6312–6317.

32 I. Pastoriza-Santos and L. M. Liz-Marzán, Colloidal silver nanoplates. State of the art and future challenges, *J. Mater. Chem.*, 2008, **18**(15), 1724–1737.

33 A. Loiseau, V. Asila, G. Boitel-Aullen, M. Lam, M. Salmain and S. Boujday, Silver-based plasmonic nanoparticles for and their use in biosensing, *Biosensors*, 2019, **9**(2), 78.

34 D. Jaque, L. Martínez Maestro, B. del Rosal, P. Haro-Gonzalez, A. Benayas, J. L. Plaza, E. Martín Rodríguez and J. García Solé, Nanoparticles for photothermal therapies, *Nanoscale*, 2014, **6**(16), 9494–9530.

35 P. Qiu and C. Mao, Seed-mediated shape evolution of gold nanomaterials: from spherical nanoparticles to polycrystalline nanochains and single-crystalline nanowires, *J. Nanopart. Res.*, 2009, **11**(4), 885–894.

36 V. Varyshchuk, T. Bulavinets, I. Yaremchuk and Y. Bobitski, The shape effect on the optical properties of metallic nanoparticles, in *2018 14th International Conference on Advanced Trends in Radioelectronics, Telecommunications and Computer Engineering (TCSET)*, IEEE, 2018, pp. 458–461.

37 C. Xue and C. A. Mirkin, pH-switchable silver nanoprism growth pathways, *Angew. Chem., Int. Ed.*, 2007, **46**(12), 2036–2038.

38 B. T. Draine and P. J. Flatau, *User guide for the discrete dipole approximation code DDSCAT 7.3*, 2013, arXiv preprint arXiv: 1305.6497.

39 J. Kelly, G. Keegan and M. Brennan-Fournet, Triangular silver nanoparticles: their preparation, functionalisation and properties, *Acta Phys. Pol., A*, 2012, **122**(2), 337–345.

40 R. Lesyuk, E. Klein, I. Yaremchuk and C. Klinke, Copper sulfide nanosheets with shape-tunable plasmonic properties in the NIR region, *Nanoscale*, 2018, **10**(44), 20640–20651.

41 R. Pązik, E. Zachanowicz, B. Pożniak, M. Małecka, A. Zięcina and Ł. Marciniak, Non-contact $Mn_{1-x}Ni_xFe_2O_4$ ferrite nano-heaters for biological applications – heat energy generated by NIR irradiation, *RSC Adv.*, 2017, **7**(29), 18162–18171.

42 E. P. Bandarra Filho, O. S. H. Mendoza, C. L. L. Beicker, A. Menezes and D. Wen, Experimental investigation of a silver nanoparticle-based direct absorption solar thermal system, *Energy Convers. Manage.*, 2014, **84**, 261–267.

43 M. Parlinska-Wojtan, J. Depciuch, B. Fryc and M. Kus-Liskiewicz, Green synthesis and antibacterial effects of aqueous colloidal solutions of silver nanoparticles using clove eugenol, *Appl. Organomet. Chem.*, 2018, **32**(4), e4276.

44 A. Regiel-Futyra, M. Kus-Liśkiewicz, V. Sebastian, S. Irusta, M. Arruebo, A. Kyzioł and G. Stochel, Development of noncytotoxic silver–chitosan nanocomposites for efficient control of biofilm forming microbes, *RSC Adv.*, 2017, **7**(83), 52398–52413.

45 M. Kus-Liśkiewicz, J. Rzeszutko, Y. Bobitski, A. Barylyak, G. Nechyporenko, V. Zinchenko and J. Zebrowski, Alternative Approach for Fighting Bacteria and Fungi: Use of Modified Fluorapatite, *J. Biomed. Nanotechnol.*, 2019, **15**(4), 848–855.

46 J. Y. Cheon, S. J. Kim, Y. H. Rhee, O. H. Kwon and W. H. Park, Shape-dependent antimicrobial activities of silver nanoparticles, *Int. J. Nanomed.*, 2019, **14**, 2773.

47 S. Pal, Y. K. Tak and J. M. Song, Does the antibacterial activity of silver nanoparticles depend on the shape of the nanoparticle? A study of the gram-negative bacterium *Escherichia coli*, *Appl. Environ. Microbiol.*, 2007, **73**(6), 1712–1720.

